



Article

3D Laser Nanoprinting of Optically Functionalized Structures with Effective-Refractive-Index Tailorable TiO₂ Nanoparticle-Doped Photoresin

Shichao Song , Yijie Li, Zhuofan Yao, Jie Li, Xiangping Li and Yaoyu Cao * 

Guangdong Provincial Key Laboratory of Optical Fiber Sensing and Communications, Institute of Photonics Technology, Jinan University, Guangzhou 511443, China; songsc@jnu.edu.cn (S.S.); liyijie@stu2018.jnu.edu.cn (Y.L.); yaozhuofan@stu2019.jnu.edu.cn (Z.Y.); tjeli@jnu.edu.cn (J.L.); xiangpingli@jnu.edu.cn (X.L.)

* Correspondence: yaoyuca@jnu.edu.cn

Abstract: The advanced direct laser printing of functional devices with tunable effective index is a key research topic in numerous emerging fields, especially in micro-/nano-optics, nanophotonics, and electronics. Photosensitized nanocomposites, consisting of high-index materials (e.g., titanium dioxide, TiO₂) embedded in polymer matrix, are emerging as attractive platforms for advanced additive manufacturing. Unfortunately, in the currently applied techniques, the preparation of optically functionalized structures based on these photosensitized nanocomposites is still hampered by many issues like hydrolysis reaction, high-temperature calcinations, and, especially, the complexity of experimental procedures. In this study, we demonstrate a feasible strategy for fabricating micro-/nanostructures with a flexibly manipulated effective refractive index by incorporating TiO₂ nanoparticles in the matrix of acrylate resin, i.e., TiO₂-based photosensitized nanocomposites. It was found that the effective refractive index of nanocomposite can be easily tuned by altering the concentration of titanium dioxide nanoparticles in the monomer matrix. For TiO₂ nanoparticle concentrations up to 30 wt%, the refractive index can be increased over 11.3% (i.e., altering from 1.50 of pure monomer to 1.67 at 532 nm). Based on such a photosensitized nanocomposite, the grating structures defined by femtosecond laser nanoprinting can offer vivid colors, ranging from crimson to magenta, as observed in the dark-field images. The minimum printing width and printing resolution are estimated at around 70 nm and 225 nm, indicating that the proposed strategy may pave the way for the production of versatile, scalable, and functionalized opto-devices with controllable refractive indices.

Keywords: titanium dioxide-based nanocomposite; optically functionalized nanostructures; laser nanoprinting; femtosecond laser; effective refractive index



Citation: Song, S.; Li, Y.; Yao, Z.; Li, J.; Li, X.; Cao, Y. 3D Laser Nanoprinting of Optically Functionalized Structures with Effective-Refractive-Index Tailorable TiO₂ Nanoparticle-Doped Photoresin. *Nanomaterials* **2022**, *12*, 55. <https://doi.org/10.3390/nano12010055>

Received: 12 November 2021

Accepted: 21 December 2021

Published: 25 December 2021

Publisher's Note: MDPI stays neutral with regard to jurisdictional claims in published maps and institutional affiliations.



Copyright: © 2021 by the authors. Licensee MDPI, Basel, Switzerland. This article is an open access article distributed under the terms and conditions of the Creative Commons Attribution (CC BY) license (<https://creativecommons.org/licenses/by/4.0/>).

1. Introduction

As one of the most common strategies used in additive manufacturing, direct-laser printing (DLP), which employs the two-photon polymerization effect, has emerged as a promising technique for fabricating spatially resolved two-dimensional (2D) or three-dimensional (3D) structures [1–5]. Featuring sub-diffraction limit resolution, DLP can offer reliable light–matter interaction at the polymerization volume [6–9]. Relying on the proper choice of photosensitized resins, various specified, multidisciplinary devices have been successfully fabricated and have evidenced their ability to deliver pre-designed functionalities [10–14], such as 3D photonics crystals [15–17], metallic structures [18–20], conductive devices [21,22], remote-responsive mechanical devices [23], etc.

Functional photosensitized nanocomposites incorporating large-index titanium dioxide (TiO₂) in photoresin matrix are regarded as beneficial material candidates for the fabrication of micro-/nano-architectures with spatially varied optical response (e.g., scattering amplitude, phase, and polarization) in the visible and near-infrared range [16,24]. General processes for the fabrication of TiO₂-based functional nanocomposites involve

deposition and etching, which limits their application, mainly in fabricating 2D structures. Currently, in most common strategies reported for direct laser printing, TiO₂-based nanostructures are demonstrated by employing liquid TiO₂ precursors and acrylic titanium alkoxide [15,25–29], both of which demand post-heat-treatment [30] for forming inorganic amorphous TiO₂ from the decomposition of organic precursors. Although an effective refractive index of TiO₂-based nanocomposite can be obtained as high as 2.3, close to the value of crystal phase [15], the post-heat-treatment may cause undesired structural shrinking [30] and poor adhesion between the sample and the substrate, which may lead to unwanted optical functionalities. In addition, tunable refractive indices can be also be produced in nanocomposites by controlling the percentage of C=C bonds consumed during the polymerization process; therefore, they could be used to produce aberration-free and plane optical surface components [31]. However, the tuning range of the refractive index still needs to be improved beyond the order of 0.01 in this method.

In this study, we demonstrate a feasible approach for fabricating micro-/nanostructures with flexibly manipulated effective refractive indices by incorporating TiO₂ nanoparticles in a matrix of acrylate resin, i.e., tailoring the TiO₂ concentration of TiO₂-based photosensitized nanocomposites. Through the implementation of this effective-refractive-index tailorable photosensitized nanocomposite, the direct printing of 3D optical nanoarchitectures can be achieved in a single attempt. For a nanocomposite with a TiO₂ concentration up to 30 wt%, the refractive index can be as high as 11.3% (i.e., increasing from 1.50 of pure monomer to 1.67 at 532 nm). As a result, the optical response of the as-fabricated micro-/nanostructures could be tuned by directly changing the TiO₂ concentration in the monomer matrix.

2. Materials and Methods

2.1. Synthesis of the Titanium Dioxide-Based Photosensitized Nanocomposites

A 3-methacryloxy propyl trimethoxy silane (MAPTMS, purchased from TCI Chemicals, Shanghai, China) is hydrolyzed in ethanol/hydrochloric acid solution (0.05 mol/L) with the weight ratio of 9:1 at 60 °C for 1 h with vigorous stirring. Next, the hydrolytic MAPTMS is added dropwise into ethanol suspension containing ~5 nm TiO₂ nanocrystals or nanoparticles (purchased from Shanghai Aladdin Biochemical Technology Co., Ltd., Shanghai, China) with vigorous stirring for 6 h. Subsequently, the TiO₂ nanoparticle sample is washed twice with ethanol to obtain the final surface-modified anatase TiO₂ nanoparticle.

2.2. Synthesis of the Photosensitized Nanocomposite Photoresin

The MAPTMS-modified TiO₂ nanoparticles are homogeneously mingled with photosensitized resin, which was composed of pentaerythritol tetraacrylate (PETTA, purchased from Sigma-Aldrich, Shanghai, China) as monomer and 0.5 wt% 7-diethylamino-3-thenoylcoumarin (DETC, purchased from Alfa Chemistry, Ronkonkoma, NY, USA) as photoinitiator.

2.3. 3D Laser Nanoprinting

The direct laser printing system is employed to produce the transdimensional structures from the TiO₂-based photosensitized nanocomposite. A 1064 nm-femtosecond laser beam, originating in the 800 nm-wavelength Ti: Sapphire laser (repetition rate of 80 MHz, pulsewidth of 140 fs, Chameleon Ultra II, Coherent, Inc., Santa Clara, CA, USA) and optical parametric oscillators (OPO) (pulse width of 210 fs, Chameleon Compact OPO, Coherent, Inc., Santa Clara, CA, USA), is used to generate the 532 nm-femtosecond laser beam with a repetition of 80 MHz and a pulse width of 210 fs through the second harmonic generator (Coherent, Inc., Santa Clara, CA, USA). The radiative 532 nm-femtosecond laser beam is directly focused onto the sample mounted on a piezo multi-axis stage (P-563.3CD, Physik Instrumente (PI) GmbH & Co. KG, Karlsruhe, Germany) through an oil immersion objective lens (UPlanSApo, 100×/1.40 (Oil), Olympus, Shinjuku-ku, Japan). A CCD camera (MER-132-43U3M-L, Daheng, Beijing, China) that provides a bright field microscope mag-

nified field of view in the visible light region is used to monitor the fabrication process of the structures.

The two-photon absorption occurs when a certain light intensity level is reached. The intensity I can be expressed as follows [32]:

$$I = \frac{2P_a T}{R\pi w_0^2 \tau} \quad (1)$$

where P_a is the average power, T is the objective transmission, R is the repetition, w_0 is the radius at the beam waist, and τ is the pulsewidth. Herein, T , R , and τ are ~ 0.85 at 532 nm, 80 MHz, and 210 fs in our 532 nm-femtosecond laser printing system, respectively. Furthermore, the optical field under tight focus effect transforms from a circular to an elliptic shape due to the depolarization. Therefore, when the polarization of the incident beam is along the y direction, the w_x and w_y are 0.1721×532 nm and 0.2449×532 nm, respectively. Consequently, the intensity I at the focal spot is calculated with the average power before pupil as $I = 2.84 \times 10^6 \cdot P_a$ ($\text{W}/\mu\text{m}^2$).

2.4. Optical Properties of the Photosensitized Nanocomposites

Since the nanocomposite is composed of host matrix and embedded nanoparticles, its optical properties can be described by an effective-medium theory [33]. The most common effective-medium theory, the Clausius–Mossoti (CM) equation, is defined as:

$$\epsilon_{\text{eff}} = \epsilon_{\text{resin}} \frac{1 + \frac{16f}{d_{\text{TiO}_2}^3} \alpha_{\text{TiO}_2}}{1 - \frac{8f}{d_{\text{TiO}_2}^3} \alpha_{\text{TiO}_2}} \quad (2)$$

where ϵ_{eff} is the effective permittivity of the nanocomposite, ϵ_{resin} is the permittivity of the host matrix, α_{TiO_2} is the dipole polarizability of the TiO_2 nanoparticles, d_{TiO_2} is the diameter of the sphere particle, $f = 4/3 \cdot N \cdot \pi (d_{\text{TiO}_2}/2)^3$ is the volume fraction, and N is the number density of the TiO_2 nanoparticles. This equation connects α_{TiO_2} to the effective permittivity of the composite (ϵ_{eff}). It is assumed that each particle can be described by a dipole moment $P_{\text{TiO}_2} = \alpha_{\text{TiO}_2} E_{\text{loc}}$, and that the local field (E_{loc}) matches the external field ($\langle E_{\text{loc}} \rangle = E_{\text{ext}}$) only when the TiO_2 nanoparticles are randomly distributed in an infinite host matrix [34,35]. However, the CM equation for the nanoparticles in a finite host matrix needs to be modified to express the polarizability α_{TiO_2} in terms of the constituents' properties, such as its size, shape, and refractive index. Thus, taking the Mie theory into account, the polarizability α_{TiO_2} can be described as [36]:

$$\alpha_{\text{TiO}_2}^{\text{Mie}} = i \frac{3(d_{\text{TiO}_2}/2)^3}{2x^3} a_1 \quad (3)$$

where a_1 is Mie coefficient of electric dipoles, and x is the size parameter ($x = \pi \cdot n_{\text{eff}} \cdot d/\lambda$, where λ is the wavelength). By substituting Equation (3) into Equation (2), the Mie-modified Maxwell–Garnett (MG) theory can be applied. If the a_1 is replaced by the expansion in Mie scattering theory, and all the first order terms are neglected, the polarizability can be simplified as in [33]:

$$\alpha_{\text{TiO}_2} = (d_{\text{TiO}_2}/2)^3 \frac{\epsilon_{\text{TiO}_2} - \epsilon_{\text{resin}}}{\epsilon_{\text{TiO}_2} + 2\epsilon_{\text{resin}}} \quad (4)$$

Next, the effective refractive index n_{eff} of this nanocomposite can be determined as:

$$n_{\text{eff}} = \sqrt{\epsilon_{\text{eff}}} \approx n_{\text{resin}} (1 + 2\pi N \text{Re}(\alpha_{\text{TiO}_2})) + i \cdot n_h 2\pi N \text{Im}(\alpha_{\text{TiO}_2}) \quad (5)$$

where n_{resin} is the refractive index of the host matrix. As a result, the scattering properties of this nanocomposite can be described by the Mie scattering theory, and the extinction (σ_{ext}) and scattering (σ_{scat}) cross-sections are:

$$\sigma_{\text{ext}}^{\text{Mie}} = \frac{\lambda^2}{2\pi} \sum_{n=0}^{\infty} (2n+1) \text{Re}(a_n + b_n) \quad (6)$$

$$\sigma_{\text{scat}}^{\text{Mie}} = \frac{\lambda^2}{2\pi} \sum_{n=0}^{\infty} (2n+1) (|a_n|^2 + |b_n|^2) \quad (7)$$

where a_n and b_n are the electric and magnetic Mie coefficients, which correspond to different multipoles ($n = 1$: dipoles; $n = 2$: quadrupoles). Furthermore, these coefficients are functions of the effective refractive index. The absorption cross section (σ_{abs}) follows from energy conservation as $\sigma_{\text{abs}} = \sigma_{\text{ext}} - \sigma_{\text{scat}}$. For dilute solutions (single scattering limit), this makes it possible to directly determine the attenuation coefficient γ , since it can be directly obtained from the imaginary part of the effective refractive index.

$$\gamma_{\text{Mie}}^{\text{ext}} = \frac{4\pi}{\lambda} \text{Im}(n_{\text{eff}}) \quad (8)$$

2.5. Measurements of Dark-Field Forward Scattering Spectrum

A home-built forward scattering measuring setup is composed of a dark-field transmission microscope (Olympus BX53, Shinjuku-ku, Japan) and a spectrometer (Andor sR500i, Oxford Instruments, Belfast, UK) mounted on the extension port. The forward scattering spectra of the samples were collected through an objective lens (MPlanFL N, $5\times/0.15$, Olympus, Shinjuku-ku, Japan). The collection angle θ of the scattering field is related to the numerical aperture NA of the objective lens, which can be described as $\theta = 2 \times \arcsin(\text{NA}/n)$, where n is the refractive index between the objective lens and the sample.

3. Results and Discussion

Due to its highly hydrophilic surface, the TiO_2 nanoparticle cannot be well dispersed in organic mediums, such as dichloromethane, methyl methacrylate. In order to improve the dispersion, the surface-modified anatase TiO_2 nanoparticles were obtained with the methods detailed in Section 2, as shown in Figure 1a. For the purpose of embedding the anatase TiO_2 nanoparticle into the photoresin homogeneously to generate the photosensitized nanocomposite, the modified TiO_2 nanoparticles/ethanol suspension was added into photosensitive resin with vigorous stirring for dispersion and ethanol evaporation, which imparted the photopolymerizable property to the TiO_2 nanoparticles. The transmission electron microscope (TEM) image, presented in Figure 1b, shows that the size of most of the MAPTMS-modified TiO_2 nanoparticles was around 5 nm. Moreover, a thin film, made of modified TiO_2 nanoparticles, was formed by volatilizing dichloromethane from the modified TiO_2 nanoparticle/dichloromethane suspension. Therefore, the spectrum captured by Fourier Transform Infrared (FTIR) Spectroscopy confirmed the successful grafting of MAPTMS organic groups on the surface of the modified TiO_2 nanoparticles, presented in Figure 1c. Consequently, as shown in Figure 1d, the photosensitized resin synthesized with functional precursors was utilized for 3D femtosecond laser prototyping to achieve the manipulation of the effective refractive index by incorporating the TiO_2 -modified nanoparticles with different concentrations into the monomer matrix.

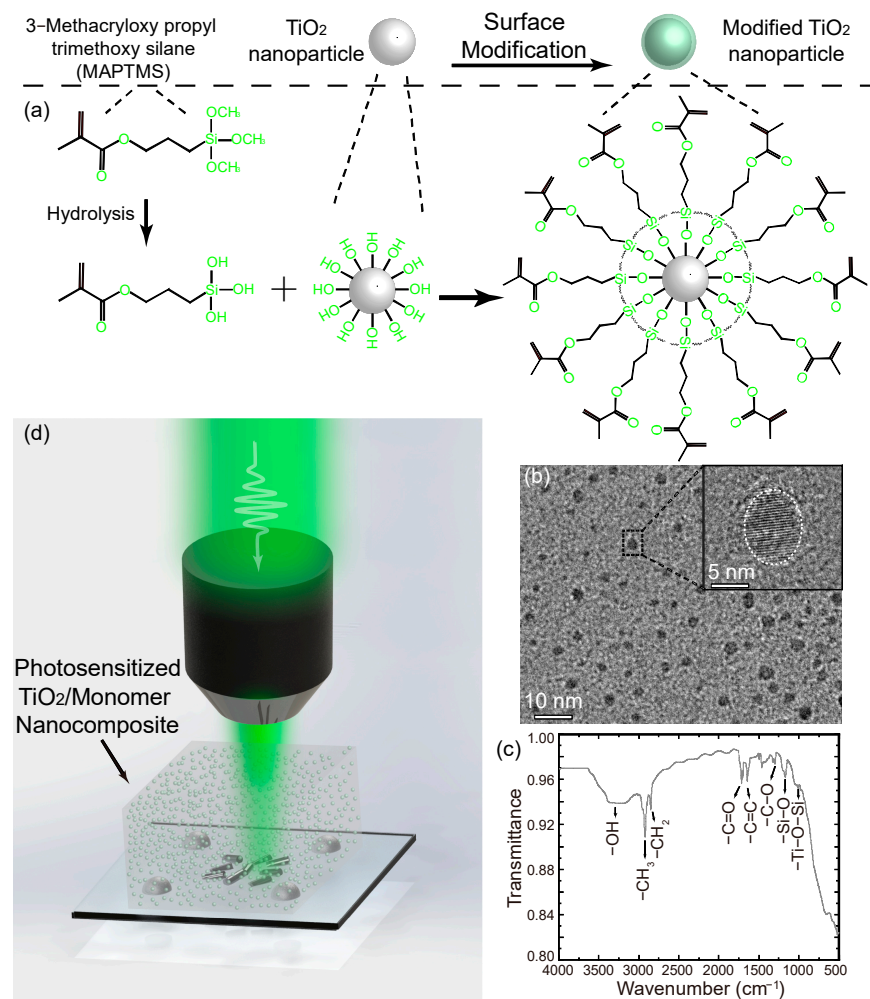


Figure 1. (a) Surface modification of TiO_2 nanoparticles with MAPTMS. (b) The TEM images of modified TiO_2 nanoparticles. (c) The FTIR spectrum of the modified TiO_2 nanoparticles. (d) Schematic of the 3D femtosecond laser nanoprining of TiO_2 -based photosensitized nanocomposites.

The 532 nm femtosecond laser beam was directly focused onto the $\sim 70 \mu\text{m}$ -thick TiO_2 -based photosensitized nanocomposite, which was sandwiched between the upper and the nether borosilicate cover slips (Fisherbrand). To further investigate the polymerization properties, a series of line structures were printed with power ranging from 1.5 to 0.4 mW, at a fixed scanning speed of $15 \mu\text{m}/\text{s}$. Scanning electron microscopy (SEM) was employed to observe and analyze the morphologies of the printed structures. The threshold power was defined as the minimum power with which the line structure can be continuously printed via the direct laser writing or the printing technique. When the weight ratio was 0 wt%, i.e., the composite was merely the photoresin; as illustrated in Figure 2a, the polymerization only occurred at power above 1.0 mW, where the linewidth was $\sim 103 \text{ nm}$. While the weight ratio varied from 10 wt% to 30 wt%, the printing threshold powers decreased from 0.8 to 0.6 mW (yellow boxes), so the single-line structures could simply be prepared with continuity. However, the predesigned line structures printed with lower powers were discrete structures consisting of isolated TiO_2 particles (blue boxes), as confirmed in Figure 2b. Thus, the line widths were measured as 80, 76, and 70 nm with weight ratios of 10–30 wt%, respectively. Consequently, benefiting from excellent photoactive properties, TiO_2 nanoparticles can serve as additional inorganic photoinitiators [37]. Therefore, with the joint contribution from these photoinitiators, the photopolymerized threshold power was reduced by 40% with the increase in the TiO_2 concentration up to 30%. Furthermore, we elaborately designed and fabricated the nanostructures with the same line width and

gradient spaces for revealing the printing resolution. Herein, printing resolution is defined as the left-edge-to-left-edge distance between two distinct adjacent lines, shown as the indicators. Furthermore, the space between the adjacent lines was designed to gradually decrease from 2 to 0.2 μm , and the rightmost gap was 0.2 μm . As presented in Figure 2c, the line width was ~ 156 nm at a power of 1.1 mW and the printing resolution was ~ 203 nm according to the indicator. When the concentration of TiO_2 nanoparticles increased to 10 wt%, as shown in Figure 2d, the line width was ~ 155 nm with a power of 0.9 mW, and the resolution was ~ 230 nm, derived from the indicator in the enlarged SEM image. While the concentration reached 20 wt%, as shown in Figure 2e, the line width was ~ 153 nm at a power of 0.8 mW; however, the rightmost lines were almost indistinguishable; the resolution was measured as ~ 235 nm at the adjacent line structures on the left, marked as the indicator. When the concentration reached 30 wt%, as presented in Figure 2f, the line width remained at ~ 152 nm, at a power of 0.7 mW. Meanwhile, the rightmost lines were completely indistinguishable; therefore, the resolution was ~ 242 nm, according to the indicator in the image. As a consequence, the printing resolution could be still maintained at ~ 235 nm despite the increase in the TiO_2 concentration.

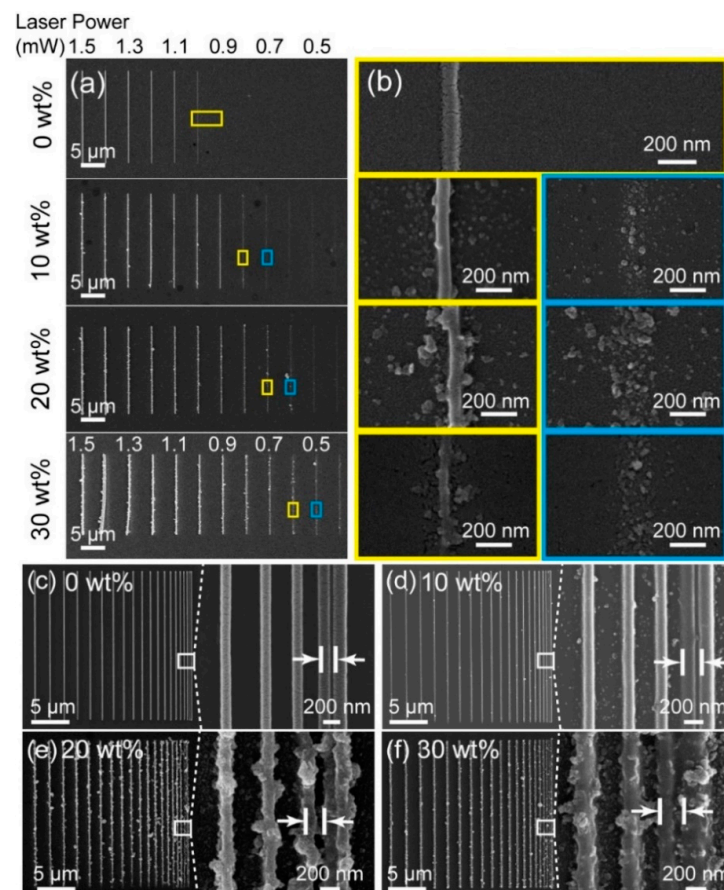


Figure 2. (a) The SEM image of the line structures at TiO_2 nanoparticle concentration of 0–30 wt% with different printing power ranging from 1.5 to 0.4 mW, respectively. (b) The enlarged structures corresponding to the yellow and blue boxes in (a). (c–f) The images relevant to the printing resolution of TiO_2 -based structures with concentrations of (c) 0 wt%, (d) 10 wt%, (e) 20 wt%, and (f) 30 wt%. The space between the adjacent lines was designed to vary from 2 to 0.2 μm . The insets illustrate the zoomed-in results of the dashed-line areas.

To investigate the optical properties of the TiO_2 -based nanocomposites, the effective refractive index n_{eff} was introduced to analyze the dispersion and optical response of the nanocomposites. The effective refractive index is closely related to the filling fraction of the

TiO₂ nanoparticles due to the Maxwell–Garnett formula in effective medium theory [34,35,38,39]; therefore, the optical properties of TiO₂-based photosensitized nanocomposites can be tailored by altering the weight ratio of TiO₂ nanoparticles. Here, we prepared four samples with different ratios of TiO₂ nanoparticles, from 0 to 30%, by spin-coating on a silicon substrate and, subsequently, UV curing. The n_{eff} of the coated nanocomposites was experimentally characterized via the ellipsometer (M-2000, J. A. Woollam Co., Lincoln, NE, USA). As depicted in Figure 3a, the measured data, fitted using the Cauchy dispersion model, confirmed that n_{eff} can be controlled over a broad range by adjusting the weight ratio. When the concentration of TiO₂ nanoparticles increased from 0% to 30%, n_{eff} increased over 11.3% (e.g., altering from 1.50 of pure monomer to 1.67 at 532 nm), which leads to spectra alterations.

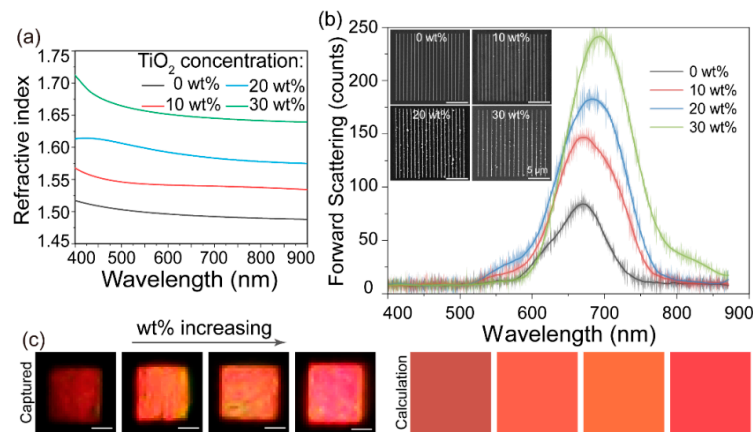


Figure 3. (a) The measured effective refractive index with four different concentrations via the ellipsometer. (b) The measured forward scattering spectra of four diffractive gratings with different concentrations. Insets: The SEM images of gratings with different TiO₂ concentrations. (c) The calculated and measured dark-field color images captured by CCD camera. All the scale bars are 5 μm.

In order to explore the spectral engineering of the as-printed nanostructures through the manipulation of n_{eff} , four diffractive gratings were printed with the period of 1.15 μm and line widths of 152 nm@1.1 mW, 154 nm@0.9 mW, 155 nm@0.8 mW, and 153 nm@0.7 mW, respectively, as shown in the insets of Figure 3b. The dark-field forward scattering spectra with approximately the same criteria were characterized with the home-built forward scattering measuring setup. These samples were illuminated with a halogen white light source through an objective lens ($\times 5$, NA = 0.15). The diffractive angles of the as-printed diffractive gratings were around $\pm 36.0^\circ$ due to the diffractive equation, while the collecting angle of the objective lens was $\pm 8.6^\circ$. Consequently, the spectra collected via the spectrometer were derived from the forward scattering of the jointed contribution of each line structure in the grating. As illustrated in Figure 3b, the collected forward scattering spectra (which can be described by the Mie scattering theory presented in Section 2) presented slight redshift and evident enhancement of scattering intensity with the gradual increase in the concentrations due to the increasing n_{eff} and effective optical path [33,35]. Moreover, the changes of the measured dark-field color images captured by the charge-coupled device (CCD) camera, shown in Figure 3c, confirm the alterations in the corresponding spectra. In addition, the calculated color images [40,41] with the measured structural and electromagnetic parameters were in good agreement with those of the experimental results. Hence, the optical activities of TiO₂-based optical functional structures can be manipulated through tailored effective refractive indices and morphological structures.

Taking full advantage of the laser printing strategy, in addition, 3D functionalized structures were fabricated to manifest the capability of the two-photon polymerization of TiO₂-based photosensitized nanocomposites. We conducted SEM and energy dispersive X-ray (EDX) analyses on the as-fabricated woodpile-like structures with the same period of 4 μm, as shown in Figure 4a. The line widths of these four woodpile-like structures

were confirmed in the zoomed-in images (insets of Figure 4a) as 156 nm@1.10 mW, 150 nm@0.89 mW, 170 nm@0.90 mW, and 162 nm@0.72 mW with the gradually increasing concentrations, respectively. Moreover, the EDX images illustrate the compositions of Ti element, which shows that the intensity increased as the concentrations of TiO₂ nanoparticles increased. This confirms that the TiO₂ nanoparticles were well embedded into the as-fabricated 3D structures. Furthermore, four hemisphere structures with different TiO₂ concentrations were used to reveal the fabrication capacity and optical properties. As presented in Figure 4b, the expected diameters were set to be 3 μ m, while the measured diameters were equal to 3.05 μ m at 0 wt%, 3.10 μ m at 10 wt%, 3.06 μ m at 20 wt%, and 3.07 μ m at 30 wt% with powers of 1.2, 1.0, 0.9, and 0.8 mW, respectively. The corresponding forward scattering spectra, illustrated in Figure 4c, indicate that the resonant wavelength redshifted and that the scattering intensity increased due to the increase in the effective optical path and n_{eff} [33,35]. Furthermore, three hemisphere structures with different diameters at the same concentration of 30 wt% were also fabricated to demonstrate the relationship between the scattering and the sizes, as depicted in Figure 4d. When the diameter varied from 1 to 3 μ m, the resonant wavelength possessed a slight redshift due to the scaling effect of optical response and the scattering intensity increased with the enlargement of the structural size. The results further confirm the capability of 3D additive manufacturing with TiO₂-based photosensitized nanocomposites, indicating its potential application in stereo-optical structures, such as spherical or aspherical lenses, 3D photonic crystals, etc.

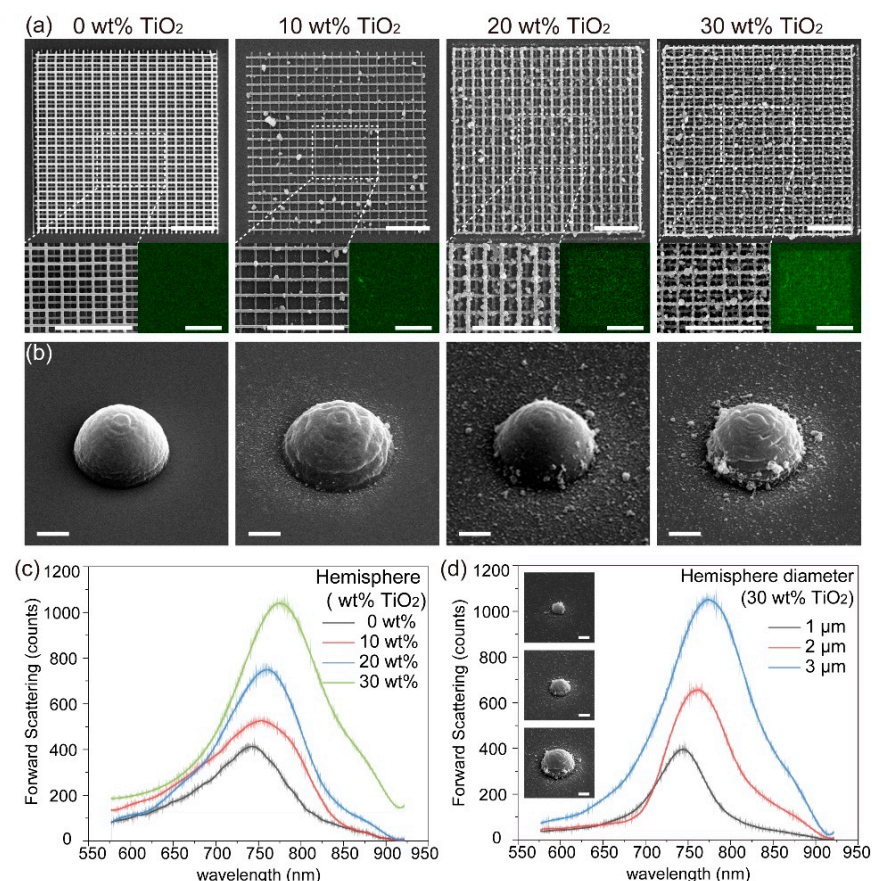


Figure 4. (a) The SEM images of the as-fabricated TiO₂-based of woodpile-like structures. Insets: the enlarged SEM imaged of the dashed boxes and compositions of Ti element. The scale bars are 5 μ m. (b) The SEM images of the as-fabricated hemispheres with expected diameters of 3 μ m. (c) The corresponding forward scattering spectra of (b). (d) The forward scattering spectra of three different hemispheres with the same concentration, 30 wt%. Insets: SEM images of corresponding hemispheres. The scale bars in (b,d) are 1 μ m.

4. Conclusions

In summary, we developed a flexible approach to generating TiO₂-based optically functionalized nanostructures with tailorable refractive indices using the laser nanoprinting technique. Fully optical direct fabrications of TiO₂-based 3D nano-architectures were achieved in a single attempt, which avoided the influence of the post-heat-treatment. The effective refractive index of the photosensitized resin could be gradually manipulated from 1.50 to 1.67 (an increment up to 11.3%) through the control of the TiO₂ concentration in the photosensitized nanocomposites. The photopolymerized threshold power could be reduced from 1.0 mW to 0.6 mW, accompanied by a reduction in the line width from ~103 to ~70 nm. Therefore, the printing resolution increased to ~235 nm due to the near-field enhancement of the TiO₂ nanoparticles. Hence, with the gradual increase in the TiO₂ concentration, the scattering spectra of the as-printed 2D and 3D structures presented redshift and increased scattering intensity, which confirmed the feasibility of the spatially varying optical response of 3D laser-printed, optically functionalized structures based on TiO₂-based photosensitized nanocomposites with tailored effective refractive indices. As a consequence, these nanocomposites could be promising candidates for producing low-threshold-polymerization-powered, large-area-miniaturized, compact, and integrated nanodevices in the fields of transdimensional optical manipulation, optical data storage, imaging, etc.

Author Contributions: Conceptualization, S.S. and Y.C.; methodology, S.S., Y.L. and Y.C.; validation, S.S., X.L. and Y.C.; formal analysis, S.S., Y.L. and Y.C.; investigation, all authors; data curation, S.S.; writing—original draft preparation, S.S.; writing—review and editing, S.S., X.L. and Y.C.; visualization, S.S. and Z.Y.; supervision, J.L., X.L. and Y.C.; project administration, Y.C.; funding acquisition, S.S., J.L., X.L. and Y.C. All authors have read and agreed to the published version of the manuscript.

Funding: This research was funded by the National Natural Science Foundation of China (NSFC) (Grant No. 61875073, 62005104), Guangdong Provincial Innovation and Entrepreneurship Project (Grant No. 2016ZT06D081), the Natural Science Foundation of Guangdong Province (Grant No. 2016A030313088), Guangdong Basic and Applied Basic Research Foundation (Grant No. 2019A1515110385), the Youth Top-Notch Scientific and Technological Innovation Talent of Guangdong Special Support Plan (Grant No. 2019TQ05X136), Zhijiang Lab (Grant No. 2020MC0AE01), and the Fundamental Research Funds for the Central Universities (Grant No. 21619339).

Institutional Review Board Statement: Not applicable.

Informed Consent Statement: Not applicable.

Data Availability Statement: The data presented in this study are available on request from the corresponding author.

Conflicts of Interest: The authors declare no conflict of interest.

References

1. Capel, A.J.; Rimington, R.P.; Lewis, M.P.; Christie, S.D.R. 3D printing for chemical, pharmaceutical and biological applications. *Nat. Rev. Chem.* **2018**, *2*, 422. [[CrossRef](#)]
2. Kiefer, P.; Hahn, V.; Nardi, M.; Yang, L.; Blasco, E.; Barner-Kowollik, C.; Wegener, M. Sensitive Photoresists for Rapid Multiphoton 3D Laser Micro- and Nanoprinting. *Adv. Opt. Mater.* **2020**, *8*, 2000895. [[CrossRef](#)]
3. Mayer, F.; Ryklin, D.; Wacker, I.; Curticean, R.; Calkovsky, M.; Niemeyer, A.; Dong, Z.Q.; Levkin, P.A.; Gerthsen, D.; Schroder, R.R.; et al. 3D Two-Photon Microprinting of Nanoporous Architectures. *Adv. Mater.* **2020**, *32*, 2002044. [[CrossRef](#)] [[PubMed](#)]
4. Kawata, S.; Sun, H.B.; Tanaka, T.; Takada, K. Finer features for functional microdevices—Micromachines can be created with higher resolution using two-photon absorption. *Nature* **2001**, *412*, 697. [[CrossRef](#)]
5. Lay, C.L.; Koh, C.S.L.; Lee, Y.H.; Phan-Quang, G.C.; Sim, H.Y.F.; Leong, S.X.; Han, X.; Phang, I.Y.; Ling, X.Y. Two-photon-assisted polymerization and reduction: Emerging formulations and applications. *ACS Appl. Mater. Interfaces* **2020**, *12*, 10061. [[CrossRef](#)] [[PubMed](#)]
6. Gan, Z.S.; Cao, Y.Y.; Evans, R.A.; Gu, M. Three-dimensional deep sub-diffraction optical beam lithography with 9 nm feature size. *Nat. Commun.* **2013**, *4*, 2061. [[CrossRef](#)]

7. Gansel, J.K.; Thiel, M.; Rill, M.S.; Decker, M.; Bade, K.; Saile, V.; von Freymann, G.; Linden, S.; Wegener, M. Gold helix photonic metamaterial as broadband circular polarizer. *Science* **2009**, *325*, 1513. [[CrossRef](#)]
8. Jiang, M.L.; Song, S.C.; Li, Y.J.; Zeng, X.Z.; Zhu, L.W.; Zhang, M.S.; Wang, S.; Li, X.P.; Cao, Y.Y. 3D high precision laser printing of a flat nanofocalizer for subwavelength light spot array. *Opt. Lett.* **2021**, *46*, 356. [[CrossRef](#)]
9. Turner, M.D.; Schroder-Turk, G.E.; Gu, M. Fabrication and characterization of three-dimensional biomimetic chiral composites. *Opt. Express* **2011**, *19*, 10001. [[CrossRef](#)]
10. Yee, D.W.; Lifson, M.L.; Edwards, B.W.; Greer, J.R. Additive manufacturing of 3D-architected multifunctional metal oxides. *Adv. Mater.* **2019**, *31*, 1901345. [[CrossRef](#)]
11. Liu, Y.J.; Wang, H.; Ho, J.F.; Ng, R.C.; Ng, R.J.H.; Hall-Chen, V.H.; Koay, E.H.H.; Dong, Z.G.; Liu, H.L.; Qiu, C.W.; et al. Structural color three-dimensional printing by shrinking photonic crystals. *Nat. Commun.* **2019**, *10*, 4340. [[CrossRef](#)]
12. Saha, S.K.; Wang, D.; Nguyen, V.H.; Chang, Y.N.; Oakdale, J.S.; Chen, S.C. Scalable submicrometer additive manufacturing. *Science* **2019**, *366*, 105. [[CrossRef](#)] [[PubMed](#)]
13. Kelly, B.E.; Bhattacharya, I.; Heidari, H.; Shusteff, M.; Spadaccini, C.M.; Taylor, H.K. Volumetric additive manufacturing via tomographic reconstruction. *Science* **2019**, *363*, 1075. [[CrossRef](#)] [[PubMed](#)]
14. Jia, Y.C.; Wang, S.X.; Chen, F. Femtosecond laser direct writing of flexibly configured waveguide geometries in optical crystals: Fabrication and application. *Opto-Electron. Adv.* **2020**, *3*, 190042. [[CrossRef](#)]
15. Vyatskikh, A.; Ng, R.C.; Edwards, B.; Briggs, R.M.; Greer, J.R. Additive Manufacturing of High-Refractive-Index, Nanoarchitected Titanium Dioxide for 3D Dielectric Photonic Crystals. *Nano Lett.* **2020**, *20*, 3513. [[CrossRef](#)] [[PubMed](#)]
16. Frolich, A.; Fischer, J.; Zebrowski, T.; Busch, K.; Wegener, M. Titania Woodpiles with Complete Three-Dimensional Photonic Bandgaps in the Visible. *Adv. Mater.* **2013**, *25*, 3588. [[CrossRef](#)] [[PubMed](#)]
17. Hossain, M.M.; Gu, M. Broadband optical absorptions in inversed woodpile metallic photonic crystals. *Opt. Mater. Express* **2012**, *2*, 996. [[CrossRef](#)]
18. Vyatskikh, A.; Delalande, S.; Kudo, A.; Zhang, X.; Portela, C.M.; Greer, J.R. Additive manufacturing of 3D nano-architected metals. *Nat. Commun.* **2018**, *9*, 593. [[CrossRef](#)]
19. Wen, H.J.; Song, S.C.; Xie, F.; Wang, B.; Xu, J.; Feng, Z.W.; Wu, S.Y.; Han, J.; Guan, B.O.; Xu, X.X.; et al. Great chiral fluorescence from the optical duality of silver nanostructures enabled by 3D laser printing. *Mater. Horiz.* **2020**, *7*, 3201. [[CrossRef](#)]
20. Xu, B.B.; Xia, H.; Niu, L.G.; Zhang, Y.L.; Sun, K.; Chen, Q.D.; Xu, Y.; Lv, Z.Q.; Li, Z.H.; Misawa, H.; et al. Flexible Nanowiring of Metal on Nonplanar Substrates by Femtosecond-Laser-Induced Electroless Plating. *Small* **2010**, *6*, 1762. [[CrossRef](#)]
21. Xiong, W.; Liu, Y.; Jiang, L.J.; Zhou, Y.S.; Li, D.W.; Jiang, L.; Silvain, J.F.; Lu, Y.F. Laser-Directed Assembly of Aligned Carbon Nanotubes in Three Dimensions for Multifunctional Device Fabrication. *Adv. Mater.* **2016**, *28*, 2002. [[CrossRef](#)] [[PubMed](#)]
22. Long, J.; Xiong, W.; Wei, C.Y.R.; Lu, C.C.F.; Wang, R.Q.; Deng, C.S.; Liu, H.; Fan, X.H.; Jiao, B.Z.; Gao, S.; et al. Directional Assembly of ZnO Nanowires via Three-Dimensional Laser Direct Writing. *Nano Lett.* **2020**, *20*, 5159. [[CrossRef](#)]
23. Xia, H.; Wang, J.A.; Tian, Y.; Chen, Q.D.; Du, X.B.; Zhang, Y.L.; He, Y.; Sun, H.B. Ferrofluids for fabrication of remotely controllable micro-nanomachines by two-photon polymerization. *Adv. Mater.* **2010**, *22*, 3204. [[CrossRef](#)] [[PubMed](#)]
24. Lu, C.L.; Yang, B. High refractive index organic-inorganic nanocomposites: Design, synthesis and application. *J. Mater. Chem.* **2009**, *19*, 2884. [[CrossRef](#)]
25. Duan, X.M.; Sun, H.B.; Kaneko, K.; Kawata, S. Two-photon polymerization of metal ions doped acrylate monomers and oligomers for three-dimensional structure fabrication. *Thin Solid Films* **2004**, *453*, 518. [[CrossRef](#)]
26. Duoss, E.B.; Twardowski, M.; Lewis, J.A. Sol-gel inks for direct-write assembly of functional oxides. *Adv. Mater.* **2007**, *19*, 3485. [[CrossRef](#)]
27. Sakellari, I.; Gaidukeviciute, A.; Giakoumaki, A.; Gray, D.; Fotakis, C.; Farsari, M.; Vamvakaki, M.; Reinhardt, C.; Ovsianikov, A.; Chichkov, B.N. Two-photon polymerization of titanium-containing sol-gel composites for three-dimensional structure fabrication. *Appl. Phys. A* **2010**, *100*, 359. [[CrossRef](#)]
28. Gorbovyi, P.; Uklein, A.; Tieng, S.; Brinza, O.; Traore, M.; Chhor, K.; Museur, L.; Kanaev, A. Novel nanostructured pHEMA-TiO₂ hybrid materials with efficient light-induced charge separation. *Nanoscale* **2011**, *3*, 1807–1812. [[CrossRef](#)] [[PubMed](#)]
29. Gorbovyi, P.; Diaz-Gomez, A.P.; Traore, M.; Museur, L.; Rozes, L.; Ribot, F.; Sanchez, C.; Kuznetsov, A.I.; Chichkov, B.N.; Kanaev, A. Alkoxysilane effect in hybrid material: A comparison of pHEMA-TiO₂ and pMAPTMS-TiO₂ nanoparticulate hybrids. *Mater. Res. Bull.* **2019**, *114*, 130. [[CrossRef](#)]
30. Gailevicius, D.; Padolskyte, V.; Mikoliunaite, L.; Sakirzanovas, S.; Juodkasis, S.; Malinauskas, M. Additive-manufacturing of 3D glass-ceramics down to nanoscale resolution. *Nanoscale Horiz.* **2019**, *4*, 647. [[CrossRef](#)]
31. Zukauskas, A.; Matulaitiene, I.; Paipulas, D.; Niaura, G.; Malinauskas, M.; Gadonas, R. Tuning the refractive index in 3D direct laser writing lithography: Towards GRIN microoptics. *Laser Photon. Rev.* **2015**, *9*, 706. [[CrossRef](#)]
32. Skliutas, E.; Lebedevaite, M.; Kabouraki, E.; Baldacchini, T.; Ostrauskaite, J.; Vamvakaki, M.; Farsari, M.; Juodkasis, S.; Malinauskas, M. Polymerization mechanisms initiated by spatio-temporally confined light. *Nanophotonics* **2021**, *10*, 1211. [[CrossRef](#)]
33. Werdehausen, D.; Staude, I.; Burger, S.; Petschulat, J.; Scharf, T.; Pertsch, T.; Decker, M. Design rules for customizable optical materials based on nanocomposites. *Opt. Mater. Express* **2018**, *8*, 3456. [[CrossRef](#)]
34. Markel, V.A. Introduction to the Maxwell Garnett approximation: Tutorial. *J. Opt. Soc. Am. A* **2016**, *33*, 1244. [[CrossRef](#)]
35. Mallet, P.; Guerin, C.A.; Sentenac, A. Maxwell-Garnett mixing rule in the presence of multiple scattering: Derivation and accuracy. *Phys. Rev. B* **2005**, *72*, 014205. [[CrossRef](#)]

36. Doyle, W.T. Optical properties of a suspension of metal spheres. *Phys. Rev. B* **1989**, *39*, 9852. [[CrossRef](#)]
37. Glass, S.; Trinklein, B.; Abel, B.; Schulze, A. TiO₂ as Photosensitizer and Photoinitiator for Synthesis of Photoactive TiO₂-PEGDA Hydrogel Without Organic Photoinitiator. *Front. Chem.* **2018**, *6*, 340. [[CrossRef](#)] [[PubMed](#)]
38. Yoon, G.; Kim, K.; Huh, D.; Lee, H.; Rho, J. Single-step manufacturing of hierarchical dielectric metalens in the visible. *Nat. Commun.* **2020**, *11*, 2268. [[CrossRef](#)] [[PubMed](#)]
39. Niklasson, G.A.; Granqvist, C.G.; Hunderi, O. Effective medium models for the optical properties of inhomogeneous materials. *Appl. Optics* **1981**, *20*, 26. [[CrossRef](#)]
40. Smith, T.; Guild, J. The C.I.E. colorimetric standards and their use. *Trans. Opt. Soc.* **1931**, *33*, 73. [[CrossRef](#)]
41. Song, S.C.; Ma, X.L.; Pu, M.B.; Li, X.; Liu, K.P.; Gao, P.; Zhao, Z.Y.; Wang, Y.Q.; Wang, C.T.; Luo, X.G. Actively Tunable Structural Color Rendering with Tensile Substrate. *Adv. Opt. Mater.* **2017**, *5*, 1600829. [[CrossRef](#)]